Plate 1.1. A facsimile reproduction of the section of the Bayeux Tapestry showing Halley's Comet in the sky above King Harold. (Courtesy of Delphine Delsemme.)

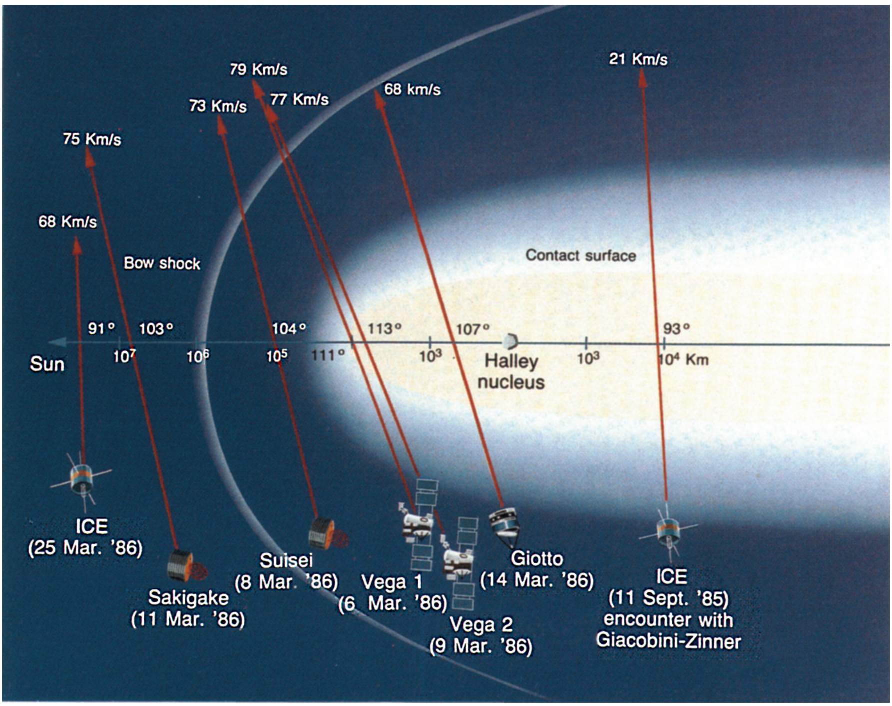

Plate 1.2. Diagrammatic summary of the spacecraft encounters with comets Halley and Giacobini–Zinner. The summary shows the dates and distances of closest approaches. The distance scale is in increments of a factor of ten. (NASA.)

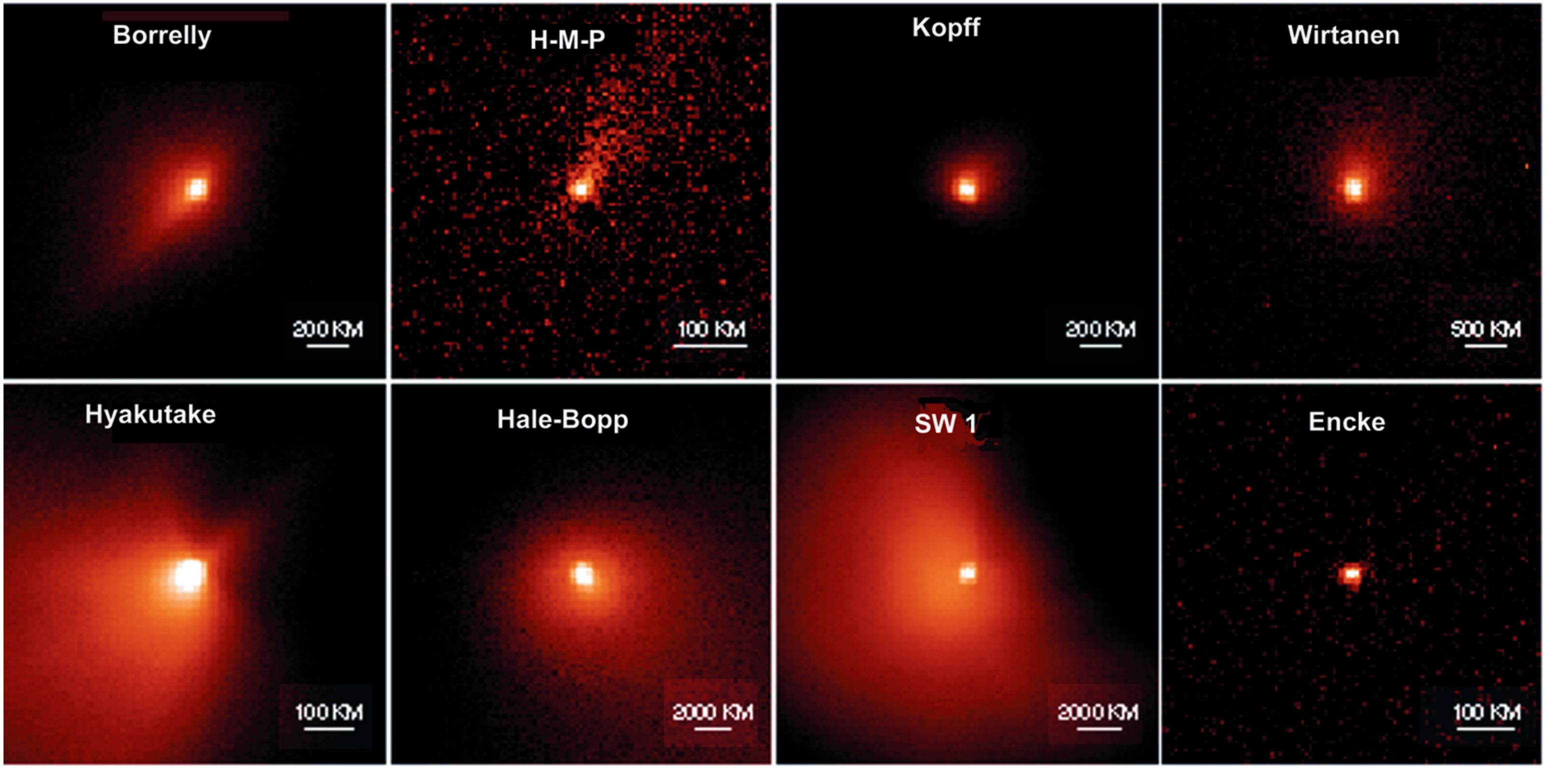

Plate 3.1. Mosaic of *HST* images of a number of the comets observed since the 1993 repair mission. (Courtesy H. Weaver.)

Plate 3.2. The Giotto fresco showing Halley's comet. © Scala/Art Resource, NY.

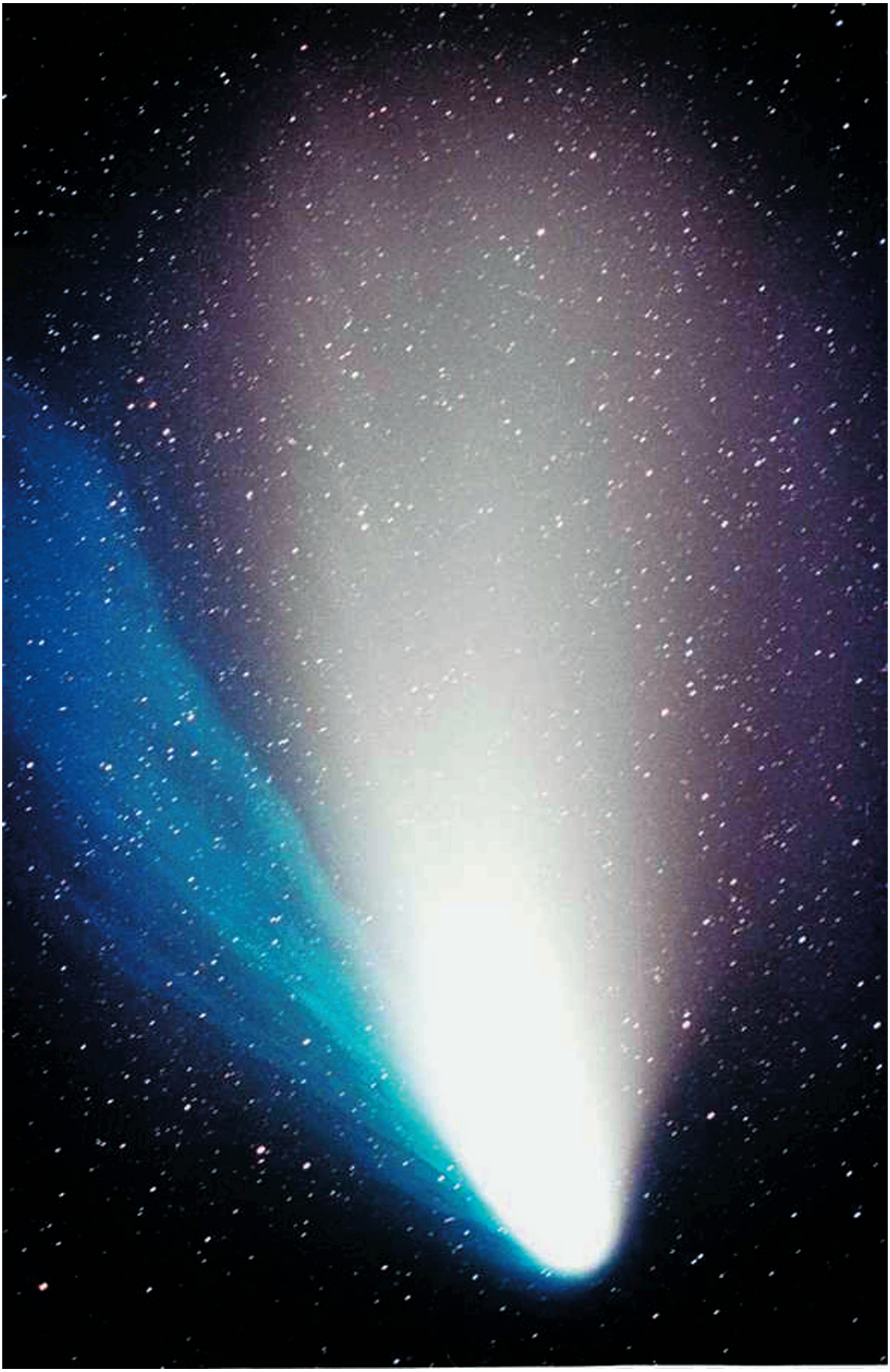

Plate 4.1. Dramatic image of comet Hale–Bopp on April 8, 1997, showing the blue plasma tail and the whitish dust tail. (Courtesy of H. Mikuz, Crni Vrh Observatory, Slovenia.)

Plate 4.2. *Infrared Astronomical Satellite* (*IRAS*) false-color image constructed from 12 μm, 60 μm, and 100 μm scans. The dust trail is the thin blue line stretching from the comet's head at upper left to the lower right. (Courtesy of Mark Sykes, University of Arizona.)

Plate 4.3. Comet Ikeya– Seki (1965f) as photographed from Kitt Peak at dawn on October 29, 1965. The yellow color is real, and is due to strong sodium emission. (Courtesy of Roger Lynds, National Optical Astronomy Observatory.)

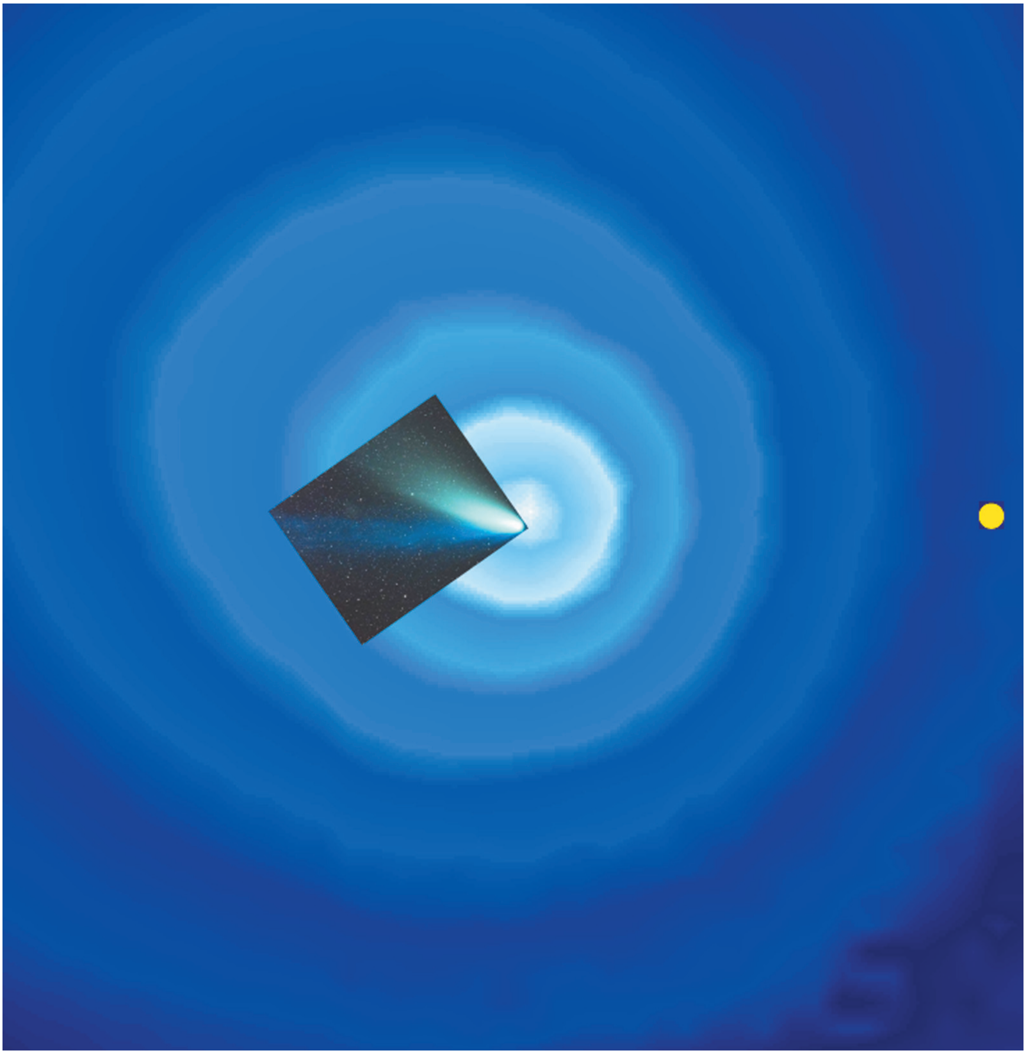

Plate 5.1. Hydrogen Lyman-α image of the coma and hydrogen cloud of comet Hale–Bopp together with a comparison with the visible ion and dust tails. The field of view is approximately 40° on a side and the image was constructed from a *SOHO* SWAN image taken on April 1, 1997, the day of perihelion. The images are to scale and the Lyman-α contours are shown in shades of blue. The small yellow disk shows the angular size of the sun and the solar direction. The visual photograph is by Dennis di Cicco and *Sky & Telescope*. (Courtesy of M. Combi, University of Michigan; see Combi *et al.* 2000.)

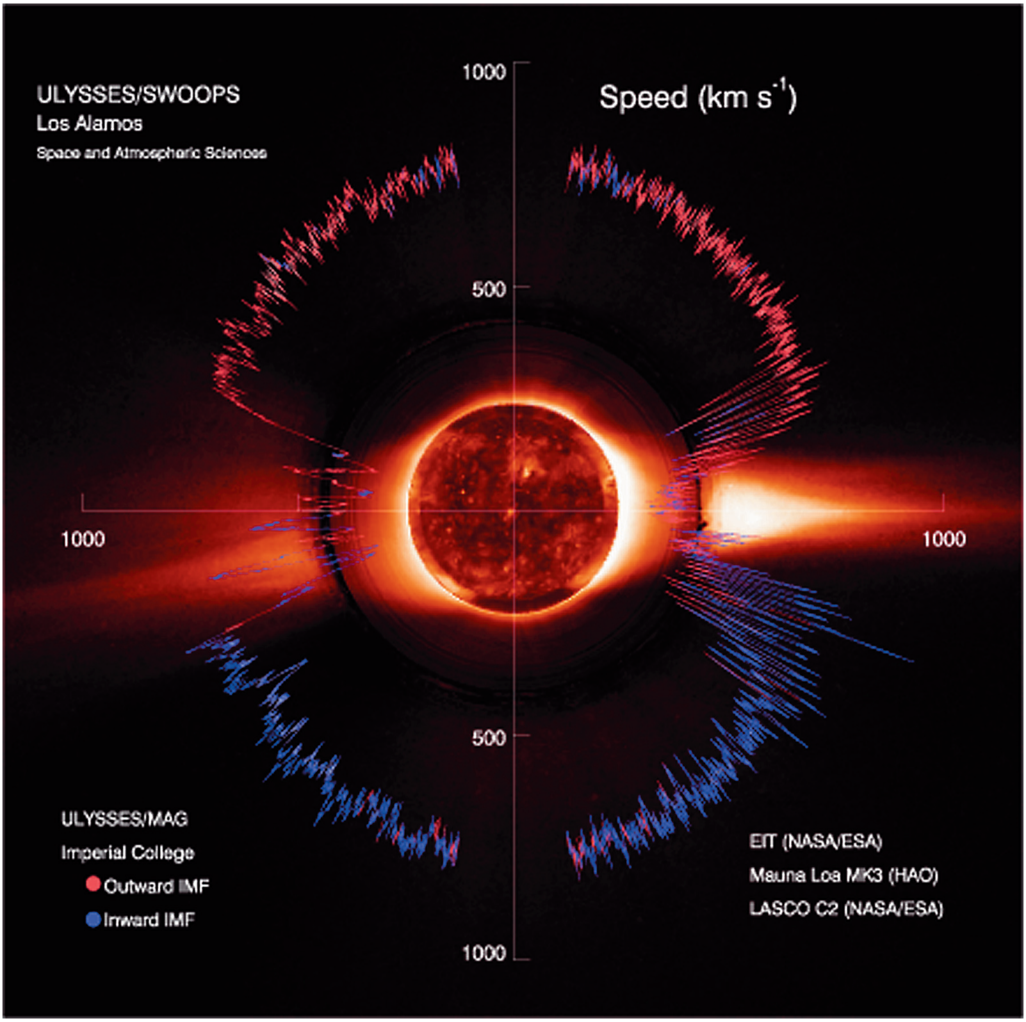

Plate 6.1. Polar plot of *Ulysses* solar-wind speeds and additional images and information as noted. The solar-wind speed of 750 km s^{-1} with small variations at polar latitudes and the solar-wind speed of 450 km s^{-1} with large variations at equatorial latitudes is clearly shown. See http://swoops.lanl.gov and McComas *et al.* 1998. (Courtesy of D. J. McComas, Southwest Research Institute.)

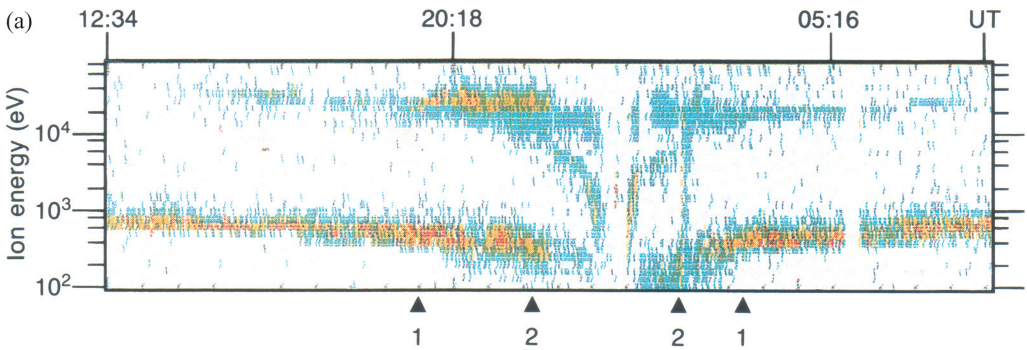

Plate 6.2. (a) Plasma results at comet Halley obtained by the ion analyzer on *Giotto*. The times refer to March 13 and 14, 1986. The data near 10^3 eV are from protons in the solar wind. The fluxes are color-coded, with red indicating the highest and dark blue the lowest. See section 6.3.2.2 for a detailed discussion. (Courtesy of the late A. Johnstone and A. Coates, Mullard Space Science Laboratory, University College London.)

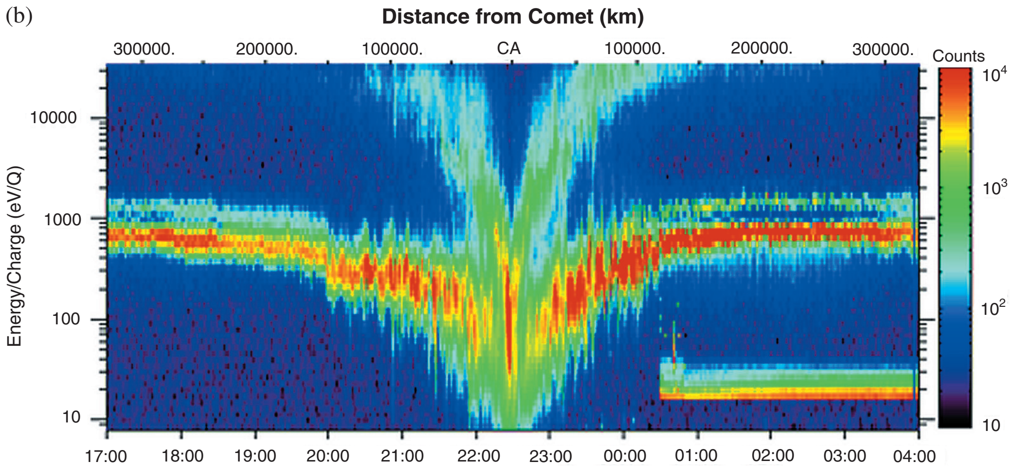

Plate 6.2. (b) Plasma results at comet Borrelly obtained by the ion analyzer on the *Deep Space 1* mission. The times refer to September 22 and 23, 2001. The bar at lower right is produced by xenon ions from the spacecraft thruster. See section 6.3.2.3 for discussion. See Nordholt *et al.* 2002. (Courtesy of Los Alamos National Laboratory.)

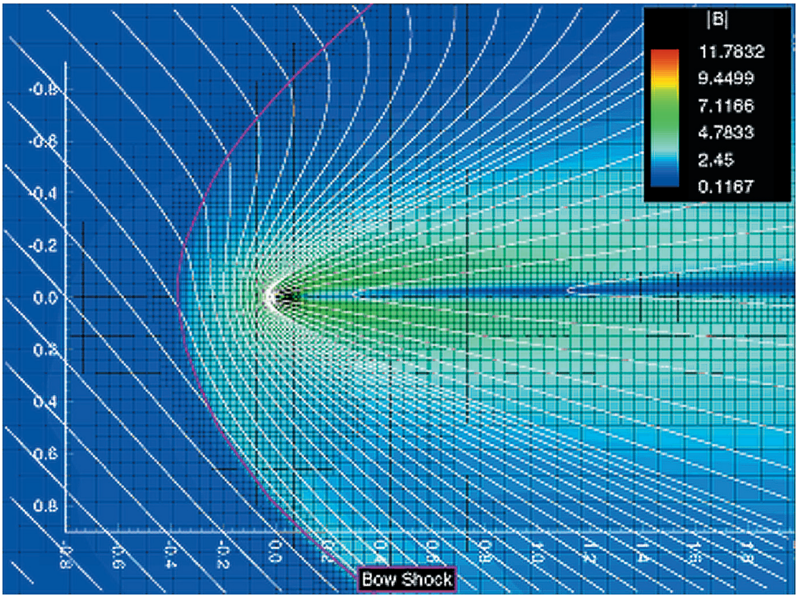

Plate 6.3. The large-scale view of model results. Approximately 2 × 3 Gm are shown. The bow shock is marked and the white lines mark the magnetic field lines in the equatorial plane (the plane of the solar wind magnetic field). The field strength is given in units of the solar-wind field, 4.81 nT. See section 6.3.3 and Gombosi *et al.* (1996). (Courtesy of T. I. Gombosi, University of Michigan, Ann Arbor.)

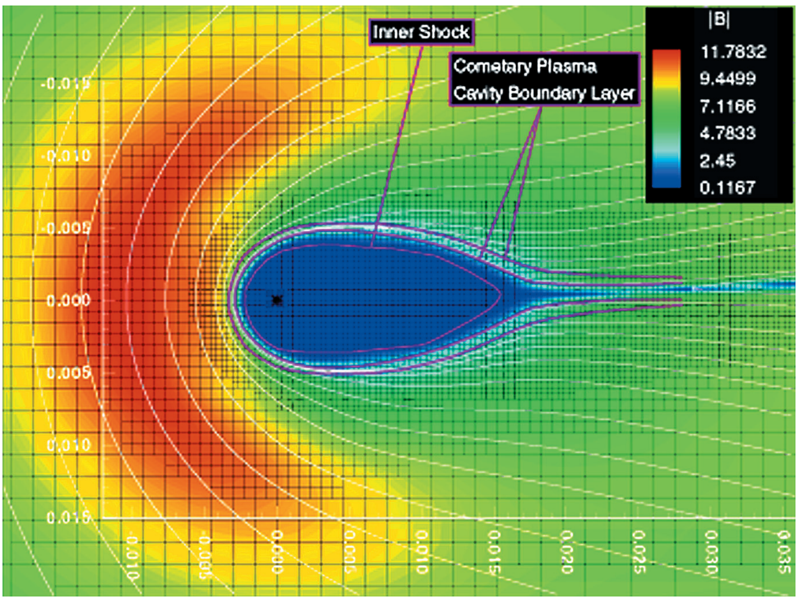

Plate 6.4. The near-nucleus view of model results. Approximately 50 000 × 30 000 km is shown. The inner shock and the diamagnetic cavity are marked. The white lines mark the magnetic field lines in the equatorial plane. The field strength is given in units of the solar-wind field, 4.81 nT. See section 6.3.3 and Gombosi *et al.* (1996). (Courtesy of T. I. Gombosi, University of Michigan, Ann Arbor.)

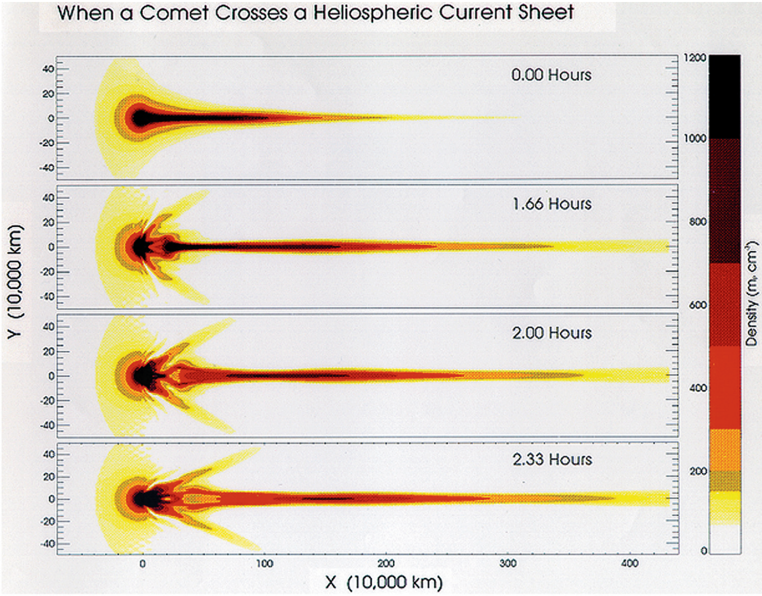

Plate 6.5. MHD simulation of a disconnection event (DE) shown in the *XY* (or equatorial) plane, the plane containing the solar wind magnetic field or IMF. The times after the polarity of the solar wind magnetic field is reversed are given. See Yi *et al.* (1996). (Courtesy of Y. Yi, Chungnam National University, South Korea.)

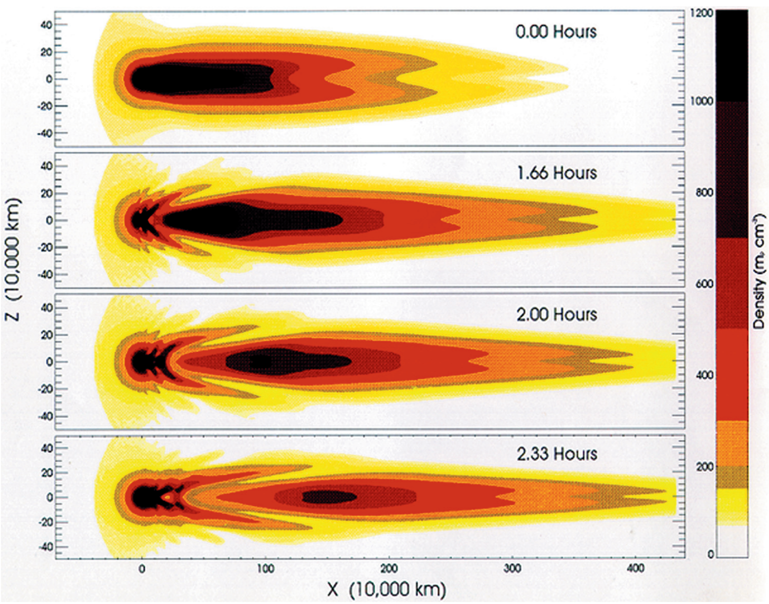

Plate 6.6. MHD simulation of a DE shown in the *XZ* plane, the plane perpendicular to the solar wind magnetic field or IMF. The times after the polarity of the IMF is reversed are given. See Yi *et al.* (1996). (Courtesy of Y. Yi, Chungnam National University, South Korea.)

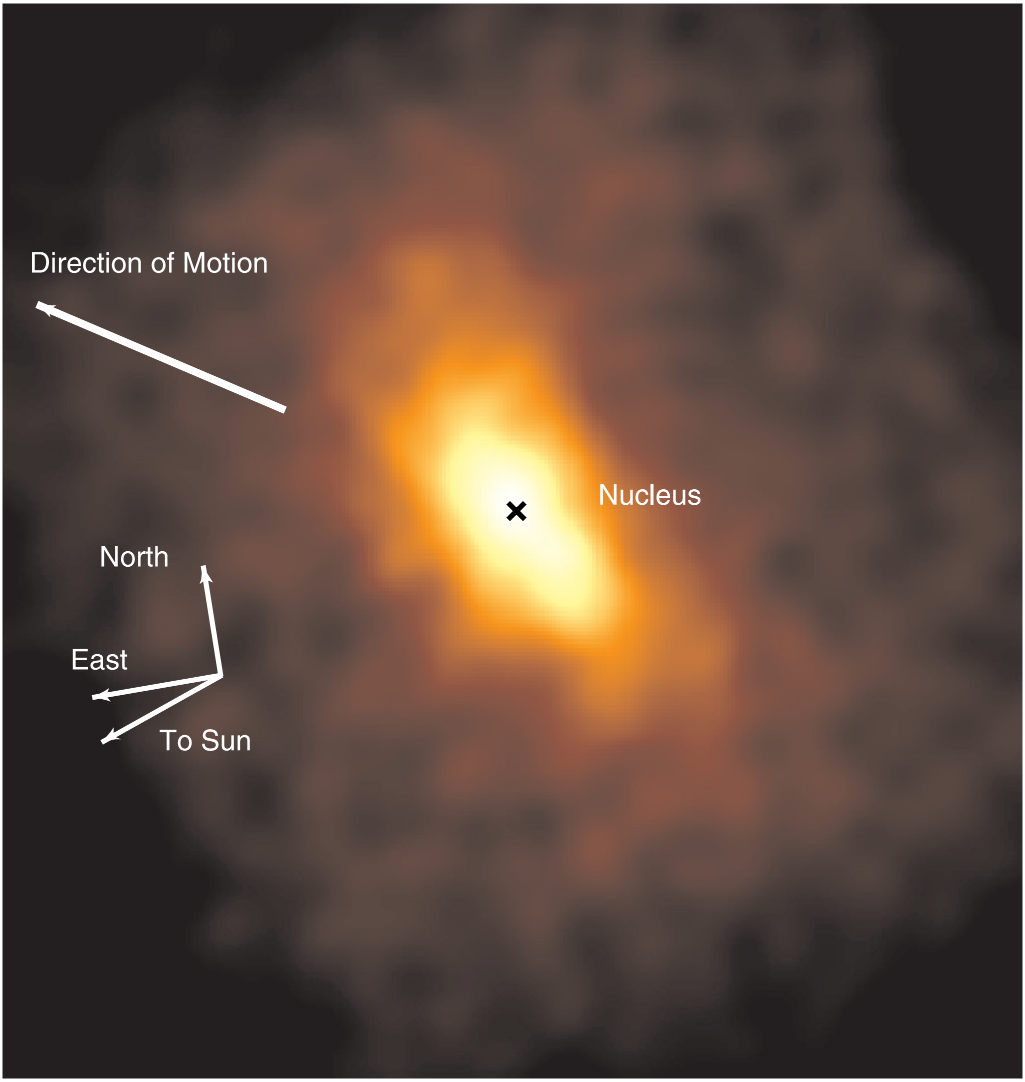

Plate 6.7. False-color representation of an x-ray (200–800 eV) image of comet LINEAR (C/1999 S4) obtained on July 14, 2000 by the Chandra X-Ray Observatory. See Lisse *et al.* (2001). (Courtesy of C. M. Lisse, University of Maryland, College Park, and S. J. Wolk, Chandra X-Ray Center, Harvard-Smithsonian Center for Astrophysics.)

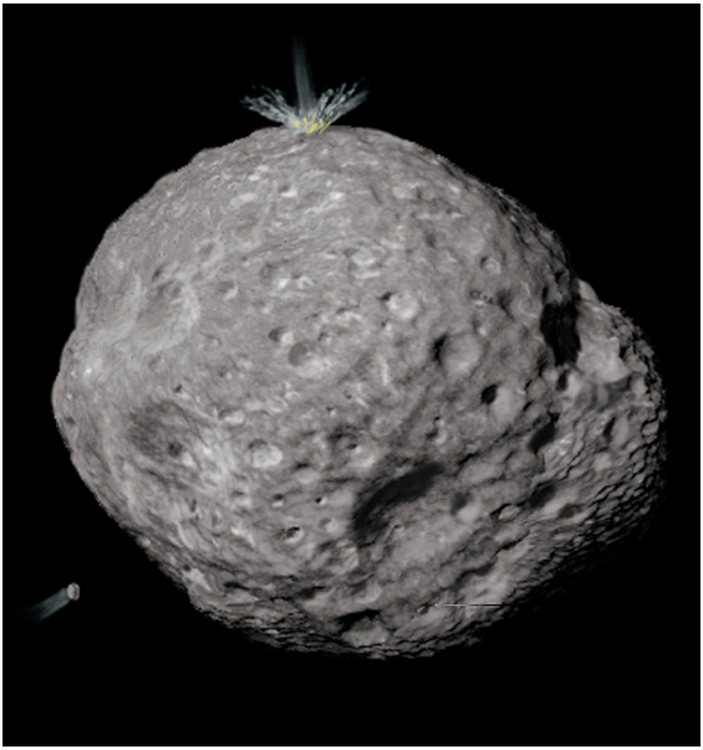

Plate 8.1. (a) Schematic of stages in the fragmentation history of a moderately large asteroid. It is originally composed of strong rock and is

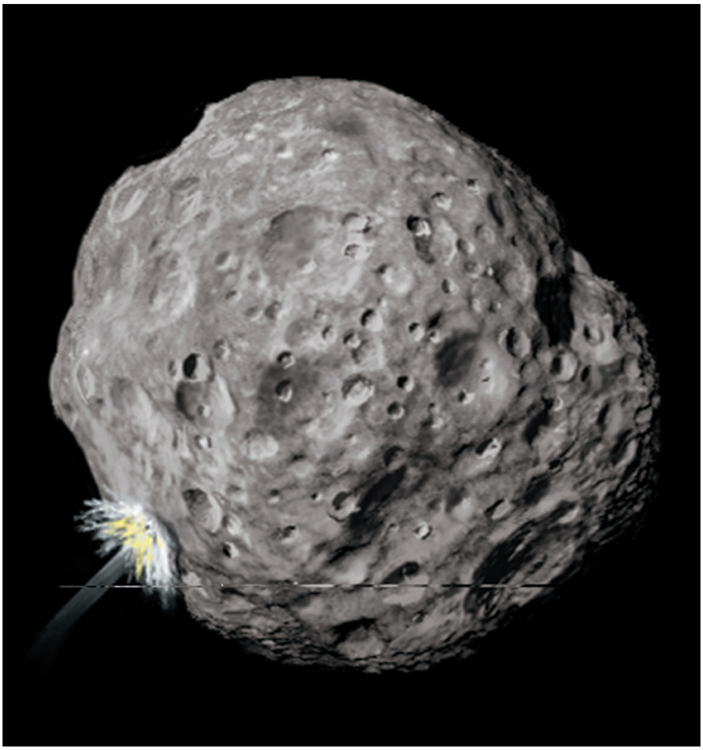

(b) cratered by impacts. An energetic impact

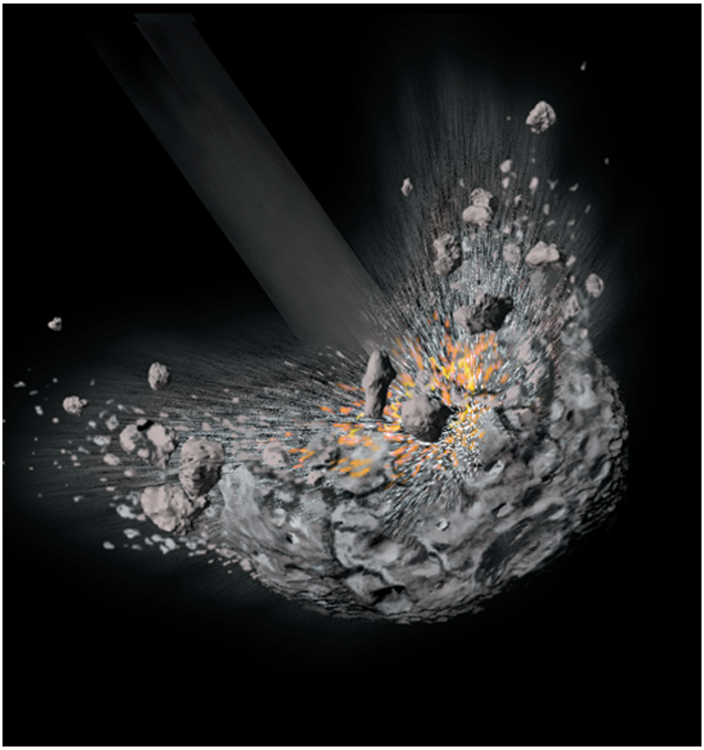

(c) totally disrupts the asteroid. Most of the fragments fail to reach escape velocity and the body reassembles.

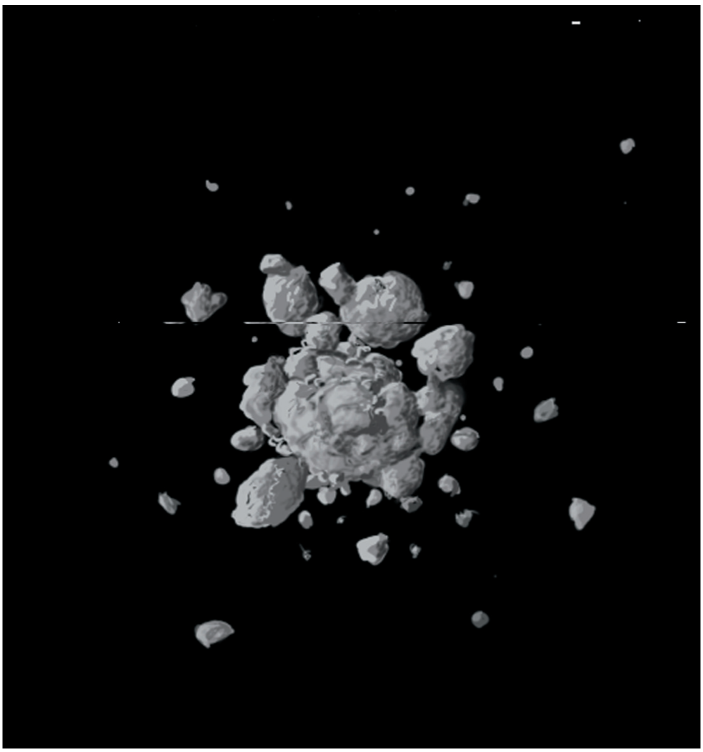

(d) Later impacts continue to fragment the body, and it is converted to a gravitationally bound pile of boulders.

(e) Finally, a gigantic collision totally disrupts the asteroid

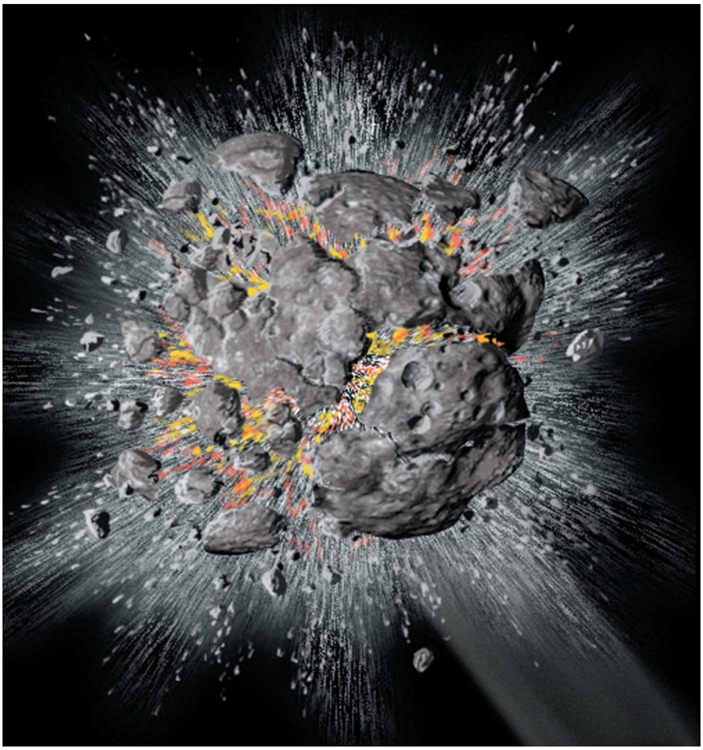

(f) and its remnants become scattered through space to form an asteroid family. (Courtesy of Don Davis/*Sky & Telescope*.)

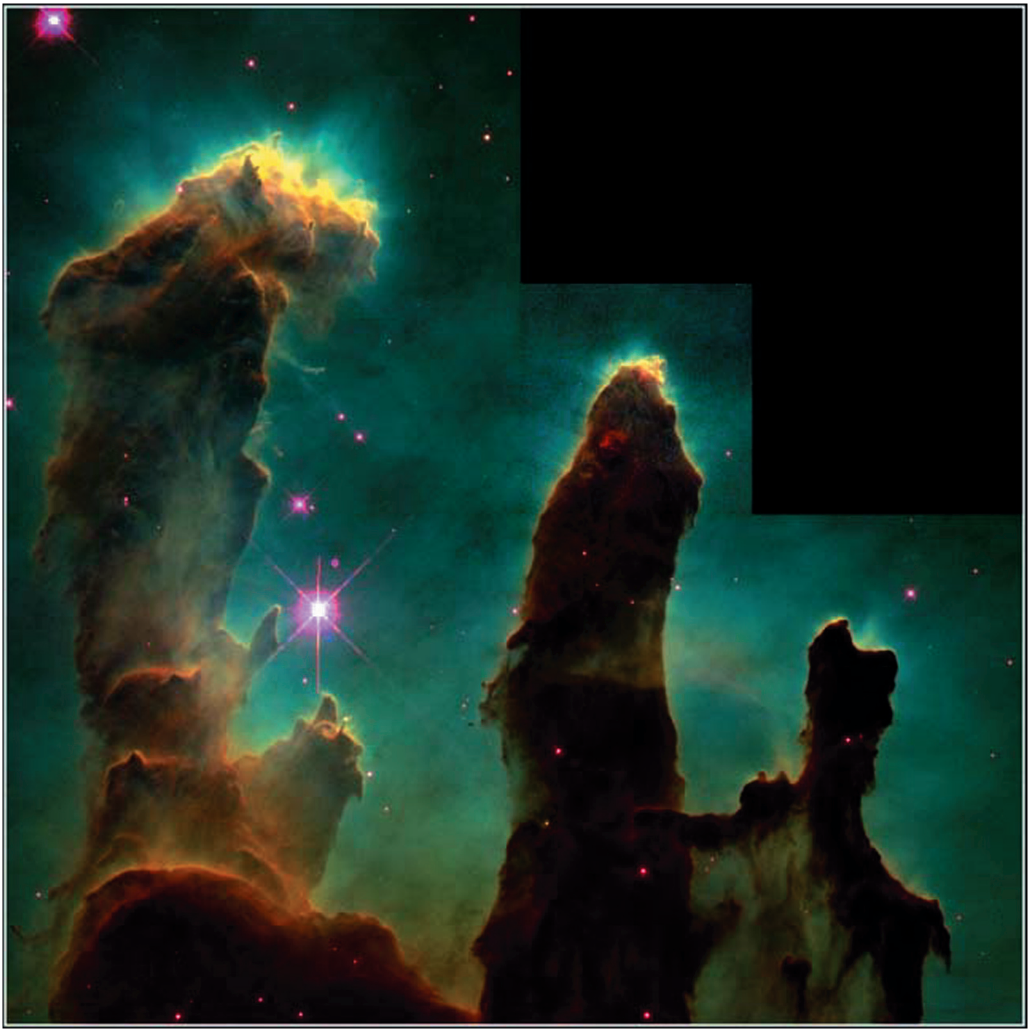

Plate 9.1. The Eagle Nebula (M16) is a region of star formation in our galaxy. (Courtesy of NASA/STScI/AURA.)

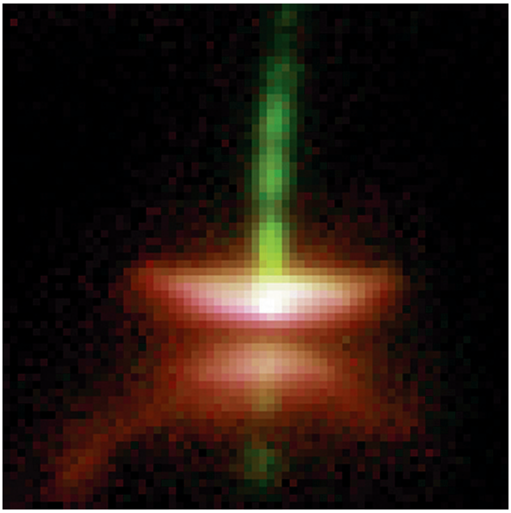

Plate 9.2. Herbig–Haro 30, a young stellar object. (*Hubble Space Telescope* (AURA/STScI/NASA).)

Plate 9.3. Tarantula Nebula complex in the Large Magellanic Cloud. The star cluster, Hodge 301 is seen in the lower right-hand corner of the image. (Hubble Heritage Team (AURA/STScI/NASA).)

Plate 10.1. *Hubble Space Telescope* image of comet Shoemaker–Levy 9 taken on May 17, 1994. The fragments of the comet extended for over 1.1 million kilometers. (Courtesy of H. A. Weaver and T. E. Smith, Space Telescope Science Institute/NASA.)

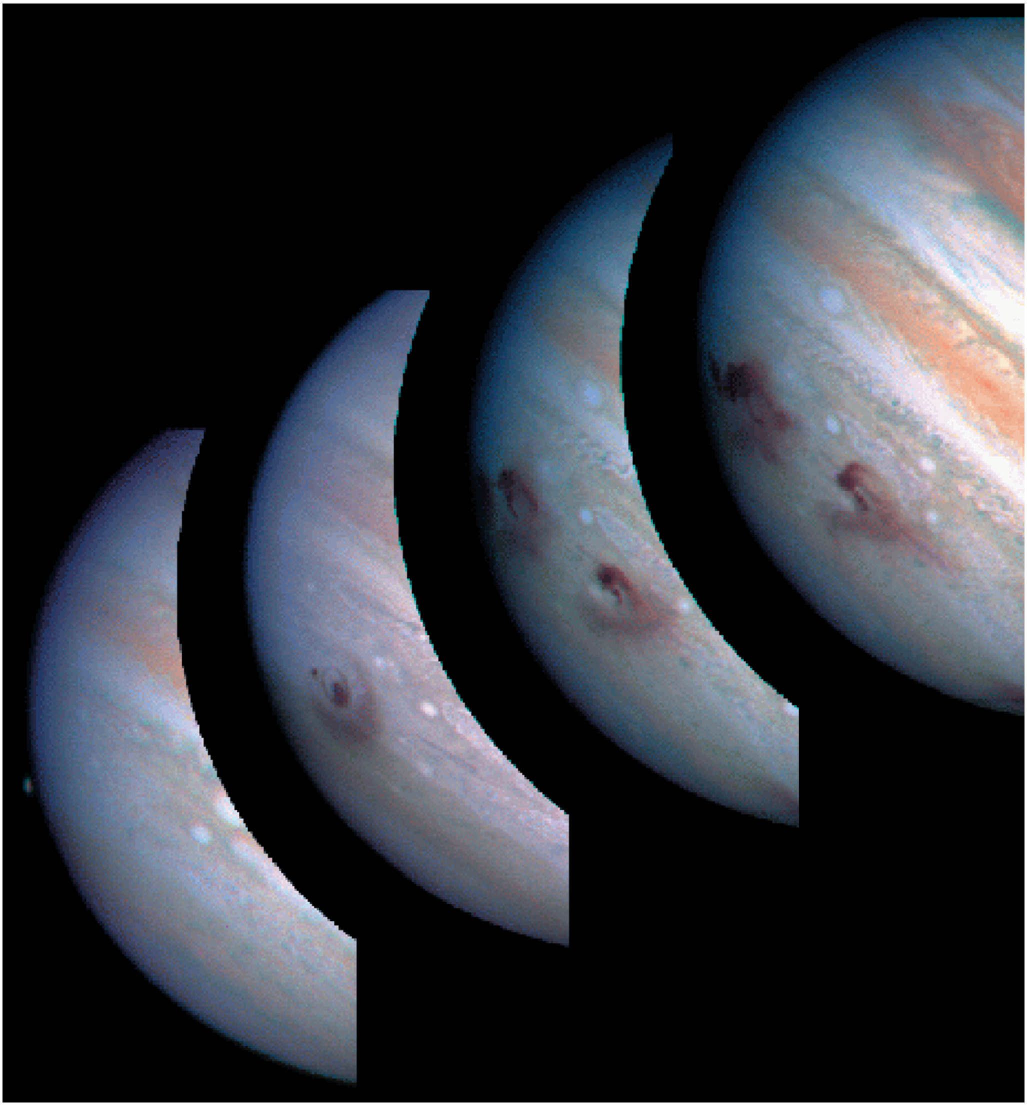

Plate 10.2. *Hubble Space Telescope* (WF/PC-2) images of the G fragment impact site. See Fig. 10.7 for a schematic. The images from lower left to upper right show: (1) The impact plume at July 18, 1994, 07:38 UT, about 5 minutes after the impact. (2) The fresh impact site at 09:19 UT, about 1.5 hours after the impact. (3) The modified impact site at July 21, 1994, 06:22 UT, about 3 days after the G impact. An additional impact is seen. (4) Further modified impact site at July 23, 1994, 09:08 UT, about 5 days after the G impact. The S impact has also occurred near the G impact site. (Courtesy of R. Evans, J. T. Trauger, H. Hammel, and the *HST* Comet Science Team/NASA.)

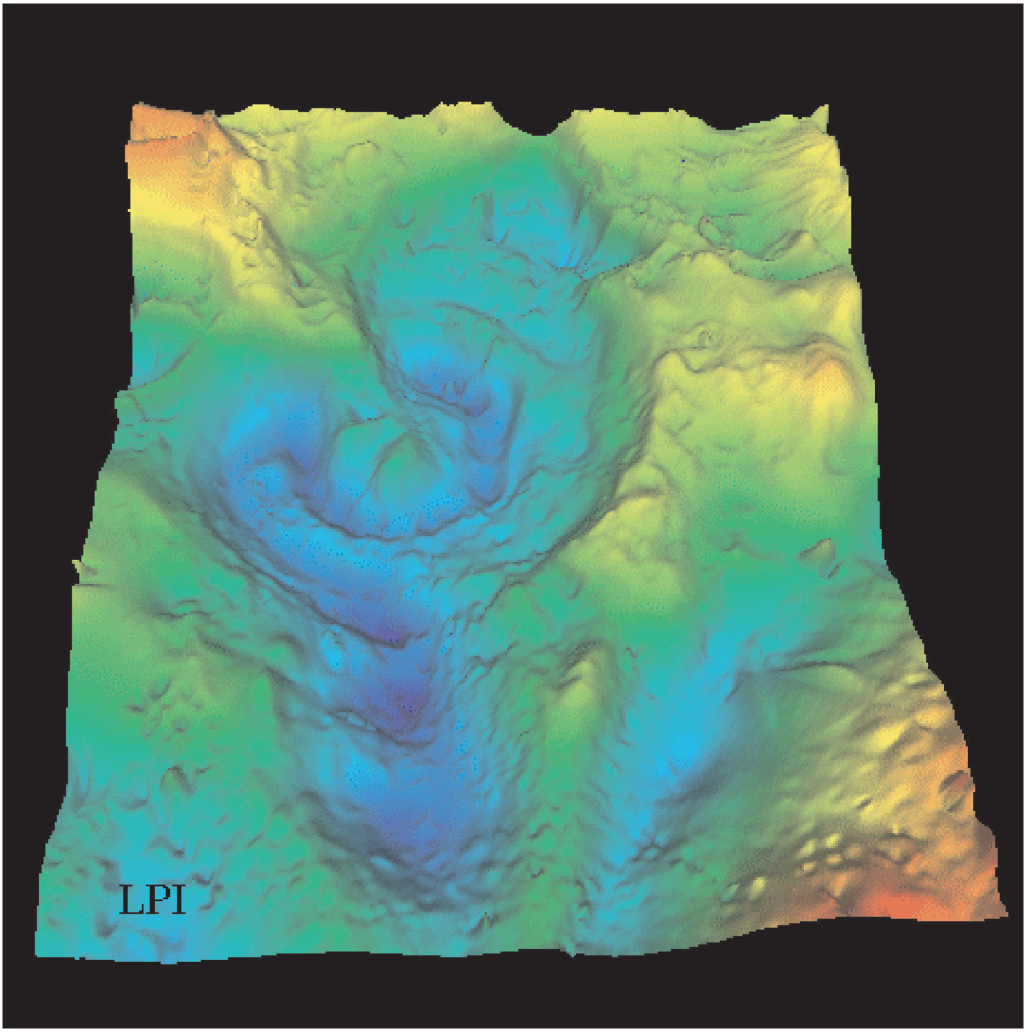

Plate 10.3. False-color representation of a gravity anomaly map of the area of the Chicxulub Crater. North is up. The crater is shown as the nearly circular, low feature in the center. The Chicxulub Crater has no central topographic feature. The other features are regional gravity anomalies and some of these (e.g., the fan shape to the north) interfere with the circular pattern. (Image by V. L. Sharpton. Courtesy: Lunar and Planetary Laboratory.)

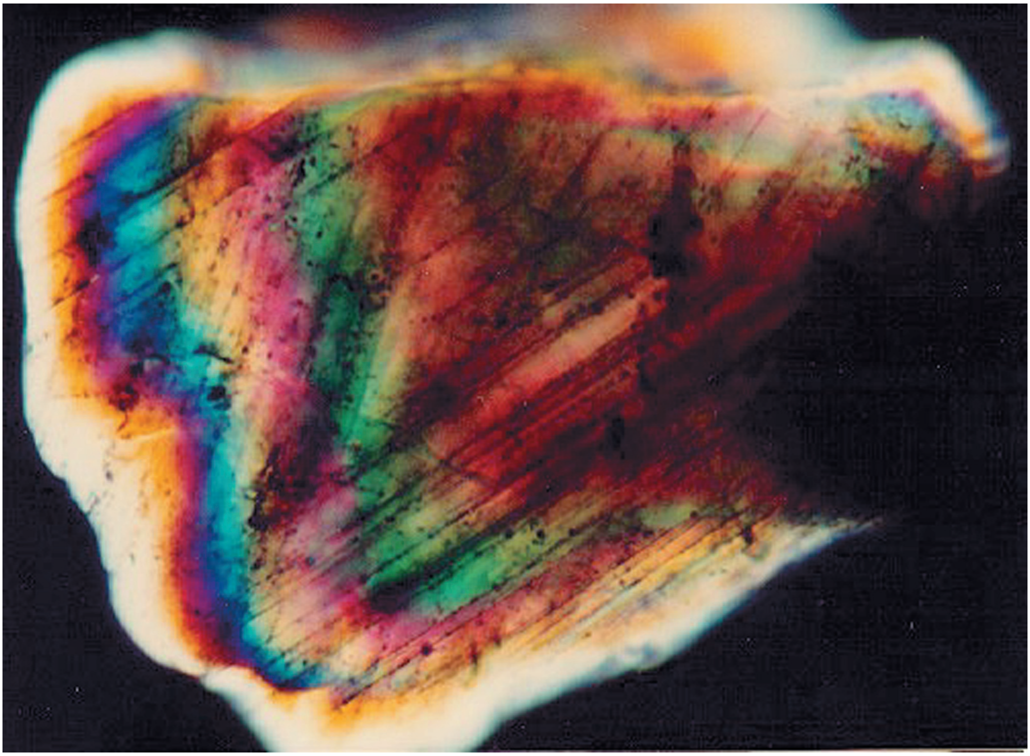

Plate 10.4. Image of a 0.32 mm shocked grain from a drill hole in the Chicxulub Crater taken in cross-polarized light. The grain shows evidence of shock metamorphism. (Courtesy of Alan Hildebrand, University of Calgary.)

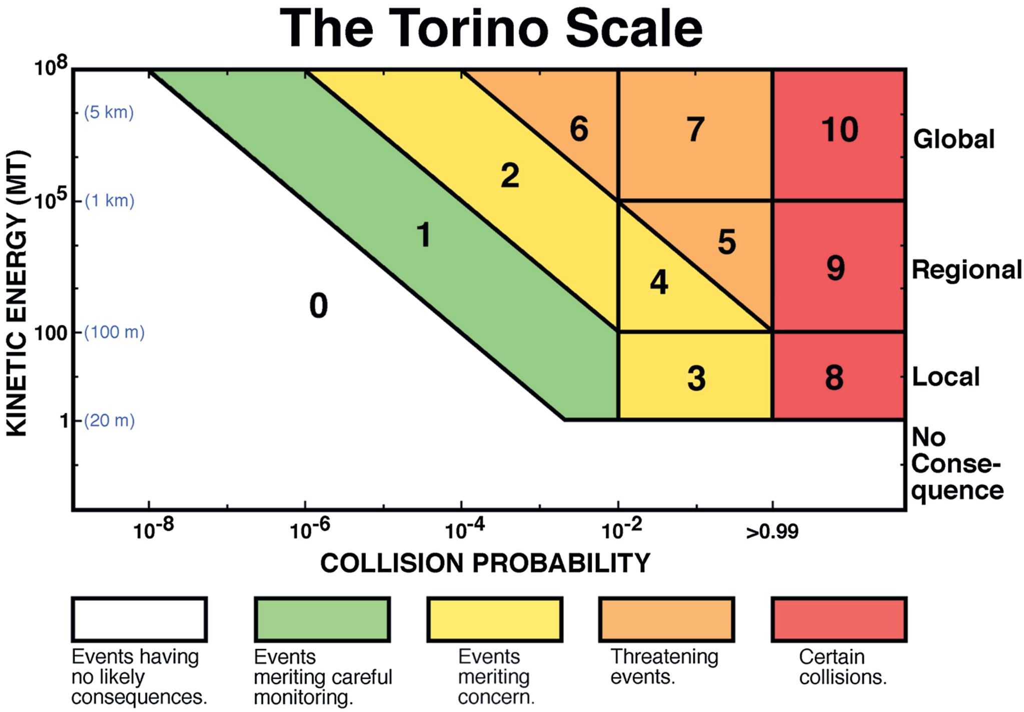

Plate 10.5. The Torino Scale Diagram. (Copyright © 1999 Richard P. Binzel, Massachusetts Institute of Technology.)

THE TORINO SCALE

Assessing Asteroid and Comet Impact Hazard Predictions in the 21st Century

Events Having No Likely Consequences	0	The likelihood of a collision is zero, or well below the chance that a random object of the same size will strike the Earth within the next few decades. This designation also applies to any small object that, in the event of a collision, is unlikely to reach the Earth's surface intact.
Events Meriting Careful Monitoring	1	The chance of collision is extremely unlikely, about the same as a random object of the same size striking the Earth within the next few decades.
Events Meriting Concern	2	A somewhat close, but not unusual encounter. Collision is very unlikely.
	3	A close encounter, with 1% or greater chance of a collision capable of causing localized destruction.
	4	A close encounter, with 1% or greater chance of a collision capable of causing regional devastation.
Threatening Events	5	A close encounter, with a significant threat of a collision capable of causing regional devastation.
	6	A close encounter, with a significant threat of a collision capable of causing a global catastrophe.
	7	A close encounter, with an extremely significant threat of a collision capable of causing a global catastrophe.
Certain Collisions	8	A collision capable of causing localized destruction. Such events occur somewhere on Earth between once per 50 years and once per 1000 years.
	9	A collision capable of causing regional devastation. Such events occur between once per 1000 years and once per 100,000 years.
	10	A collision capable of causing a global climatic catastrophe. Such events occur once per 100,000 years, or less often.

Plate 10.6. Explanation of the Torino Scale. (Copyright © 1999 Richard P. Binzel, Massachusetts Institute of Technology.)

Plate 12.1. Comet Halley over the Thames in 1759 as painted by Samuel Scott. (Smithsonian Institution Archives.)

Plate 12.2. Halley postage stamps.